Landsat-5 TM Reflective-Band Absolute Radiometric Calibration

Gyanesh Chander, Dennis L. Helder, *Member, IEEE*, Brian L. Markham, *Member, IEEE*, James D. Dewald, *Member, IEEE*, Ed Kaita, Kurtis J. Thome, Esad Micijevic, and Timothy A. Ruggles, *Member, IEEE*

***Abstract*—The Landsat-5 Thematic Mapper (TM) sensor provides the longest running continuous dataset of moderate spatial resolution remote sensing imagery, dating back to its launch in March 1984. Historically, the radiometric calibration procedure for this imagery used the instrument's response to the Internal Calibrator (IC) on a scene-by-scene basis to determine the gain and offset of each detector. Due to observed degradations in the IC, a new procedure was implemented for U.S.-processed data in May 2003. This new calibration procedure is based on a lifetime radiometric calibration model for the instrument's reflective bands (1–5 and 7) and is derived, in part, from the IC response without the related degradation effects and is tied to the cross calibration with the Landsat-7 Enhanced Thematic Mapper Plus. Reflective-band absolute radiometric accuracy of the instrument tends to be on the order of 7% to 10%, based on a variety of calibration methods.**

***Index Terms*—Absolute calibration, characterization, Internal Calibrator (IC), Landsat, Landsat-5 (L5) Thematic Mapper (TM), Landsat-7 (L7) Enhanced Thematic Mapper Plus (ETM+), lookup table (LUT), radiance, radiometry, reflectance, relative spectral response, vicarious.**

I. Introduction

THE LANDSAT program began in 1972 and has since provided continuous, consistent measurements of earth surface features over seven mission generations. Landsat sensors have been developed specifically to detect and quantify changes in the earth's environment and its global energy balance. Two such satellites in near-polar orbit, Landsat-4 and Landsat-5, carry the Thematic Mapper (TM) sensor. When launched, these satellites marked a significant advance in remote sensing through the addition of an enhanced sensor system, an increased data acquisition and transmission capability, and more rapid data processing at highly automated facilities. Although L5 was launched in March 1984, it continues operating to this day, far beyond its expected five-year lifetime. Nevertheless, the instrument has aged, and its characteristics have changed since its launch. These changes must be adequately characterized and corrected, if possible, to preserve the usefulness of the acquired data.

L5 was developed and launched in 1984 by the National Aeronautics and Space Administration (NASA). Following on-orbit testing, L5 was turned over to the National Oceanic and Atmospheric Administration (NOAA). In September 1985, NOAA transferred operational control of L5 to a commercial vendor, the Earth Observation Satellite (EOSAT) Company (currently known as Space Imaging, Inc). In July 2001, operational control of L5, and its entire data archive, was returned to the U.S. Government, to be administered by the U.S. Geological Survey (USGS).

Three data product generation systems have been used to process L5 image data in the U.S. The first processing system, used by NOAA and adopted later by EOSAT, was the TM Image Processing System (TIPS). EOSAT updated TIPS to the Enhanced Image Processing System (EIPS) in October 1991. At the same time, the USGS began work on its own TM archive, processing TM data with the National Landsat Archive Production System (NLAPS), created by MacDonald Dettwiler Associates (MDA).

A. Instrument Overview

The orbit of Landsat-5 is repetitive, circular, sun-synchronous, and near polar at a nominal altitude of 705 km (438 miles) at the equator. The spacecraft crosses the equator from north to south on a descending orbital node from between 10:00 A.M. and 10:15 A.M. on each pass. Circling the earth at 7.5 km/s, each orbit takes nearly 99 min. The spacecraft completes just over 14 orbits per day, covering the entire earth between 81° north and south latitude every 16 days. The TM instrument provides image data with eight-bit radiometric resolution in seven bands covering the visible, near infrared, shortwave infrared and thermal regions of the electromagnetic spectrum. Bands 1–4 use 16-element Si-based detector arrays with center wavelengths of 0.49, 0.56, 0.66, and 0.83 μm. Bands 5 and 7 use 16-element, cooled InSb-based detector arrays with center wavelengths of 1.67 and 2.24 μm. Band 6, the thermal emissive band, uses a cooled four-element HgCdTe-based array with a center wavelength of around 11.5 μm. The six reflective

Manuscript received November 30, 2003; revised May 29, 2004. This work was supported in part by the National Aeronautics and Space Administration Landsat Project Science Office under Dr. D. Williams, Project Scientist, and in part by the U.S. Geological Survey Earth Resources Observation System Data Center Land Remote Sensing Program under Wayne Miller and Tracy Zeiler, Project Chiefs.

G. Chander and E. Micijevic are with the Science Application International Corporation, Earth Resources Observation System Data Center, U.S. Geological Survey, Sioux Falls, SD 57198 USA (e-mail: gchander@usgs.gov).

D. L. Helder, J. D. Dewald, and T. A. Ruggles are with the Electrical Engineering and Computer Science Department, South Dakota State University, SD 57007 USA (e-mail: Dennis.Helder@sdstate.edu).

B. L. Markham is with the Landsat Project Science Office, NASA Goddard Space Flight Center, Greenbelt, MD 20771 USA (e-mail: Brian.L.Markham@nasa.gov).

E. Kaita is with the Science Systems and Applications, Incorporated, NASA Goddard Space Flight Center, Greenbelt, MD 20771 USA (e-mail: Edward.Kaita@gsfc.nasa.gov).

K. J. Thome is with the Remote Sensing Group, Optical Sciences Center, University of Arizona, Tucson, AZ 85721 USA (e-mail: kurt.thome@opt-sci.arizona.edu).

Digital Object Identifier 10.1109/TGRS.2004.836388

TABLE I
L5 TM SPECTRAL COVERAGE AND GROUND SAMPLE DISTANCE [1]

Band	Type	Spectral range (μm)		GSD (m)
1	Si Photodiode	Blue-Green	0.450-0.520	30
2	Si Photodiode	Green	0.520-0.600	30
3	Si Photodiode	Red	0.630-0.690	30
4	Si Photodiode	Near-IR	0.760-0.900	30
5	InSb	Mid-IR1	1.550-1.750	30
6	HgCdTe	Thermal-IR	10.40-12.50	120
7	InSb	Mid-IR2	2.080-2.350	30

bands have a spatial resolution of 30 m, and the thermal band has a spatial resolution of 120 m. Table I provides a summary of some of the key characteristics of these instruments, including the spectral range of the channels [1].

The TM sensor incorporates an onboard radiometric calibration system called the Internal Calibrator (IC), which is located in front of the primary focal plane. The IC has a shutter flag that includes optical components that direct light from three lamps, located near the base of the shutter flag, to the detectors. The output from each lamp is modified by a different attenuation filter, producing three different intensities that can be combined into eight distinct brightness levels. The lamps are continuously cycled through an eight state sequence during a 24-s scene acquisition, and their outputs are monitored by unfiltered silicon photodiodes located behind a hole in the condenser mirrors within the lamp assemblies; the lamp currents are controlled by feedback networks such that the photodiode outputs remain constant. The shutter flag oscillates in synchronization with the scan mirror such that, at the end of each image scan, the shutter flag obscures the primary focal plane (and by extension the cold focal plane, through an optical relay system), blocking reception of reflected scene energy. The shutter flag is painted black and provides both focal planes with a zero-radiance reference [2].

B. Purpose of This Paper

Teams from the Image Assessment System (IAS), Landsat Project Science Office (LPSO), Canada Centre for Remote Sensing (CCRS), South Dakota State University (SDSU), University of Arizona (UOA), Jet Propulsion Laboratory (JPL), Rochester Institute of Technology (RIT), MacDonald Dettwiler Associates (MDA), and others involved in Landsat calibration meet on a semiannual basis to compare results from independent calibration efforts. For the L5 TM, the current emphasis is on determining the calibration history for the entire archive and making recommendations for necessary corrections. The ultimate goal of these calibration teams has been to characterize the instrument and provide accurate radiometric calibration for any point in its lifetime. This paper focuses on the calibration of the reflective bands of the L5 TM instrument.

A revised radiometric calibration of the L5 TM sensor for its entire mission has been developed and anchored to that of the L7 ETM+. This paper documents the results of the collaborative effort on an improved calibration procedure and provides specifications for the related calibration algorithms. This paper includes: 1) development of lifetime calibration equations; 2) refinements to calibration models accounting for outgassing effects; 3) revised postcalibration dynamic range; 4) lookup table (LUT) implementation of absolute gains generated from time-dependent models; 5) operational implementation of revised calibration procedures; and 6) improvement in calibration consistency of L5 with L7. A more detailed treatment of the development of the lifetime gain equations is provided in Teillet *et al.* [3]. A succinct treatment of the information users need with equations and parameters for converting the digital numbers (DNs) from the image data to useful quantities such as spectral radiance (L_λ) and top-of-atmosphere (TOA) reflectance (ρ_P) or temperature (T) estimates is provided in [4] and [5].

Historically, L5 TM calibration information has been presented in spectral radiance units of milliwatts per square centimeter per steradian per micron. To maintain consistency with L7 ETM+, this paper uses spectral radiance units of watts per square meter per steradian per micron; note that the conversion factor is $1:10$ when going from one radiance unit to the other.

II. L5 TM ARTIFACT CORRECTIONS

This paper deals primarily with the development of a calibration procedure for determining a single gain value per band for a scene of data. A number of other issues need to be dealt with to maintain the internal consistency of the calibration within a scene. These include artifact correction and detector-to-detector normalization. This section reviews these effects.

A. Artifacts

Radiometric performance studies of the L4/L5 TM sensors have led to a detailed understanding of several image artifacts due to particular sensor characteristics. These artifacts were observed in image data shortly after launch of the L4 TM. Before radiometric calibration of the Landsat TM data can be done accurately, it is necessary to minimize the effects of these artifacts in the data, originating in the instrument's signal processing path. Data analysis has identified three primary radiometric artifacts: scan-correlated shift (SCS), coherent noise (CN), and memory effect (ME). All three are normally difficult to observe except in fairly homogeneous regions such as water or desert. To varying degrees, they have also been observed in calibration data. Other secondary artifacts have been observed; however, their effects on image data are significantly smaller.

SCS is a sudden, simultaneous shift in the bias level of all detectors occurring at the end of a scan line; all detectors shift at the same time between two bias levels. It is easily corrected in image data simply by subtracting bias from each scan line. Coherent noise is a periodic noise pattern that is present in all imagery. The noise level is very low, typically less than one DN. ME is a significant problem that can cause, in the worst case, an 8-DN error in pixel intensity. This problem is due to the response of a first-order resistance–capacitance network within the analog preamplifiers used by bands 1–4.

Additional information on TM artifacts and the correction procedures can be found in the TM on-orbit radiometric performance [6].

TABLE II
L5 TM PRELAUNCH GAIN/BIAS COEFFICIENTS [8]

Band	Prelaunch Gain	Prelaunch Bias
1	1.555	1.8331
2	0.786	1.6896
3	1.02	1.8850
4	1.082	2.2373
5	7.875	3.2893
7	14.77	3.2117

TABLE III
LIFETIME VICARIOUS CALIBRATIONS AND GAIN COEFFICIENTS IN DIGITAL NUMBERS PER UNIT RADIANCES WATTS PER SQUARE METER PER STERADIAN PER MICRON FOR THE DATES SHOWN FOR THE SIX SOLAR REFLECTIVE BANDS OF L5 TM BASED ON LEVEL 0R DATA

L5 TM Vicarious Calibration Gain							
Prelaunch		B1	B2	B3	B4	B5	B7
		1.555	0.786	1.020	1.082	7.875	14.770
DOY	Year						
UAZ		B1	B2	B3	B4	B5	B7
190	84	0.000	0.734	0.955	1.055	0.000	0.000
301	84	1.389	0.732	0.927	1.087	7.024	14.990
144	85	0.000	0.749	0.942	1.045	0.000	0.000
240	85	0.000	0.715	0.914	1.121	7.227	15.240
320	85	1.367	0.716	0.922	1.094	7.506	16.110
86	87	1.307	0.702	0.891	1.048	7.441	16.180
41	88	1.304	0.721	0.918	1.059	7.351	16.290
227	92	0.000	0.651	0.883	1.048	7.416	15.450
294	93	1.281	0.683	0.924	1.094	7.477	15.240
281	94	1.222	0.653	0.887	1.054	6.811	13.170
351	96	1.201	0.631	0.883	1.042	5.759	15.040
81	97	0.000	0.589	0.838	1.046	7.382	12.080
145	97	0.000	0.645	0.910	1.111	7.873	14.640
69	98	1.232	0.629	0.892	1.073	7.829	14.080
78	98	1.214	0.615	0.889	1.115	8.170	14.720
170	98	1.261	0.645	0.916	1.138	8.004	14.580
145	99	1.165	0.586	0.858	1.064	7.874	14.430
152	99	1.211	0.627	0.895	1.111	8.097	14.850
SDSU		B1	B2	B3	B4	B5	B7
153	99	1.221	0.662	0.904	0.980	7.681	16.910
155	99	1.183	0.631	0.860	1.049	7.316	12.895
187	99	1.294	0.692	0.884	1.023	7.739	15.213
267	99	1.210	0.627	0.870	0.988	7.684	13.960
174	2000	1.309	0.675	0.929	1.032	7.542	15.038
190	2000	1.275	0.697	0.977	1.037	7.988	17.603
222	2000	1.289	0.659	0.922	1.074	7.902	16.679
Cross cal with L7		B1	B2	B3	B4	B5	B7
152	99	1.243	0.656	0.905	1.082	7.944	14.520

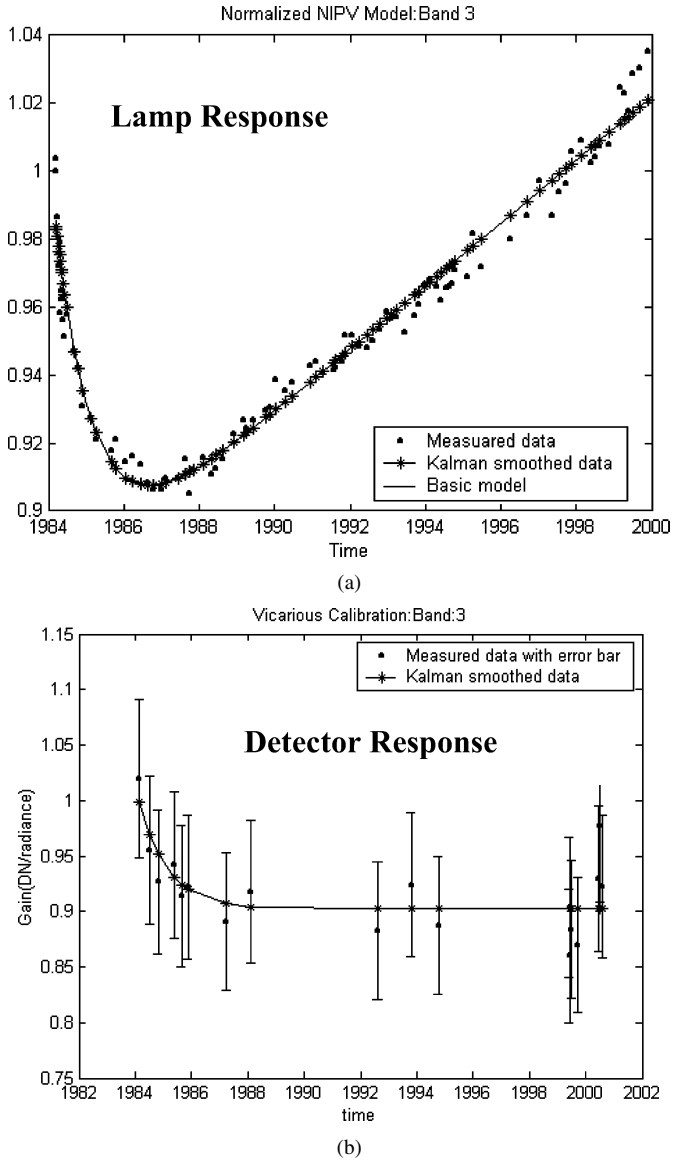

Fig. 1. (a) Normalized net pulse value and (b) the detector response (gain) in units of DN/radiance.

B. Detector Equalization

Individual detectors within an array typically do not possess similar gain and bias characteristics. This mismatch of detector response results in the appearance of striping in acquired images. Striping has been the most significant radiometric artifact observed in all of the Landsat imaging sensors, beginning with the Multispectral Scanner (MSS) on Landsat-1 in 1972. It is also clearly evident in TM imagery. The objective of detector equalization, or "relative" radiometric calibration, is to reduce striping effects by establishing a reference, based on a single detector or a band average of all detectors, and then shifting and scaling the detector responses to match the reference gain and bias level [7]. One method of achieving this equalization is histogram equalization, which is discussed below.

1) Histogram Equalization: A destriping algorithm was developed at CCRS for the MSS on Landsat-1 and was improved and adapted to the TM sensor by Murphy (1984). This algorithm has been incorporated into the Landsat Level 1 Product Generation System (LPGS), Product Generation System (PGS), Thematic Mapper Bulk Processing System (TMBPS), and Geometric Image Correction System (GICS). On a scene-specific basis, it determines the bias and gain of each detector relative to a reference detector and then equalizes the detectors to the bias and gain of the reference. In most U.S. implementations, the reference detector is typically a "pseudo"-detector whose gain and bias are the arithmetic mean of the gains and biases of all detectors. Canadian implementations, on the other hand, choose a single detector as the reference.

C. Icing Corrections for Bands 5 and 7

The detectors of bands 5, 6, and 7 are located on the cold focal plane (CFP) at a temperature maintained between 95–105 K, to minimize thermal noise and allow adequate detection of scene energy. Gain oscillations observed in bands 5 and 7 are believed to be caused by ice that builds up on the window of a dewar that

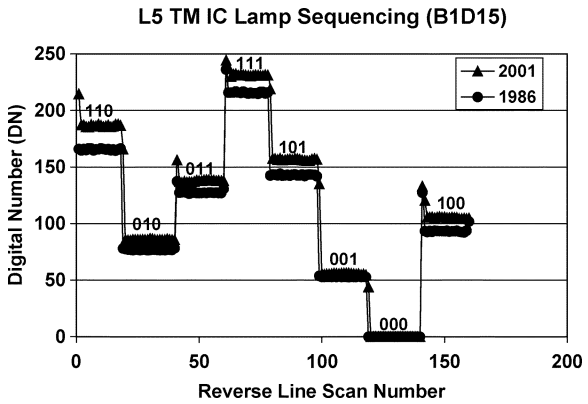

Fig. 2. L5 TM IC lamp sequencing for band 1 detector 15.

houses the CFP detectors. This process of icing, an effect of outgassing, is detected and characterized through observations of IC data, revealing an indication of 3% to 5% uncertainty in absolute gain estimates. Correction of the gain oscillations makes use of a thin-film interference model developed at SDSU. The model is based on an analysis of closely sampled sets of detector responses from the TM's lifetime and relates detector behavior to both the accumulated ice thickness, since the previous outgassing event and the current growth rate of the ice film. This model provides correction coefficients on a daily basis for any point in time since the launch of the satellite [6].

III. L5 TM Absolute Radiometric Calibration

The Landsat series of satellites has provided the longest running continuous dataset of moderate spatial-resolution imagery, dating back to the launch of Landsat-1 in 1972. Part of the success of the Landsat program has been the ability to understand the radiometric properties of its various sensors. This understanding is attributed to a combination of prelaunch and postlaunch data from laboratory, onboard, and vicarious calibration methods. Radiometric calibration of these sensors helps characterize the operation of the instrument, but more importantly, the calibration allows the full Landsat data archive to be used in a quantitative sense.

A. Prelaunch Instrument Gain

Prelaunch calibration of the sensors is the work done in the laboratory before the instrument's launch. It allows the system to be tested to ensure it operates properly before being integrated into the launch vehicle. Laboratory calibrations are easier to control and perform than methods used after launch. During the preflight phase, TM detectors were calibrated using a secondary standard integrating sphere (IS122 of the U.S. National Bureau of Standards). Several calibration tests have been carried out under ambient and vacuum conditions. Tables containing fixed estimates of detector gain and bias for each TM detector are provided in the Landsat to Ground Station Interface Description document [8]. This document also provides radiance levels for each calibration lamp configuration as sensed by each single detector given in digital counts, which are related to effective radiance by the gain and bias values.

TABLE IV
Comparison of Tandem-Orbit-Based (RVPN Xcal) and Vicarious (RVPN UOA) Calibration Results for Landsat 5 TM Gain Coefficients for the RVPN Test Site in June 1999. A Comparison Between RVPN Xcal and Prelaunch Gain Coefficients Is Also Included. Gains Are in Units of Watts per Square Meter per Steradian per Micron [16]

Spectral Band	RVPN Xcal	RVPN UAZ	% Diff re Xcal		RVPN Xcal	Prelaunch Calibration	% Diff re Prelaunch
1	1.243	1.211	-2.60%		1.243	1.555	-20.0%
2	0.6561	0.627	-4.40%		0.6561	0.786	-16.5%
3	0.905	0.8953	-1.10%		0.905	1.02	-11.3%
4	1.082	1.111	+2.70%		1.082	1.082	0%
5	7.944	8.097	+1.9 %		7.944	7.875	+0.88 %
7	14.52	15.26	+5.1 %		14.52	14.77	-1.7 %

TABLE V
Coefficients for Time-Dependent Characterization of L5 TM Lifetime Gain Based on IC Trend Analysis, Anchored to L7 ETM+ via Cross Calibration Using the Tandem-Orbit Image Pair for RVPN in 1999. Coefficients a_0 and a_2 Are in Units of Watts per Square Meter per Steradian per Micron and the a_1 Coefficients Are Dimensionless

Spectral Band	a_0	a_1	a_2
1	0.1457	0.9551	1.243
2	0.05865	0.8360	0.6561
3	0.1119	1.002	0.9050
4	0.1077	1.277	1.0820
5	0.2545	1.093	7.944
7	0.4967	0.9795	14.52

Before its launch, L5 was well-calibrated radiometrically. However, following launch, the IC response of the instrument decreased in an exponential manner due to spectral filter outgassing. Table II summarizes the prelaunch gain and bias coefficients. The prelaunch gain coefficients are not consistent with the vicarious and onboard calibrations performed throughout the instrument's lifetime. A large variation, on the order of 20%, has been observed between the prelaunch values and postlaunch cross-calibration and vicarious calibration values. As such, the prelaunch gain coefficients are not useful for performing radiometric calibration, and it has been recommended that the International Ground Stations (IGSs) update their processing systems from the default database values to the revised definitive gain coefficients.

B. Lifetime Vicarious Calibration Gains

As previously mentioned, the internal calibrator is incorporated as an onboard radiometric calibration system. Vicarious calibration is an approach that attempts to estimate the radiance seen at the sensor (basically at the top of the earth's atmosphere) over a selected test site on the earth's surface, using *in situ* measurement results and radiative transfer code computations. The onboard lamp systems provide a high-precision view of the sensor's behavior as a function of time, over time intervals ranging from a single orbital period to several months. For longer time intervals, it becomes necessary to verify the status

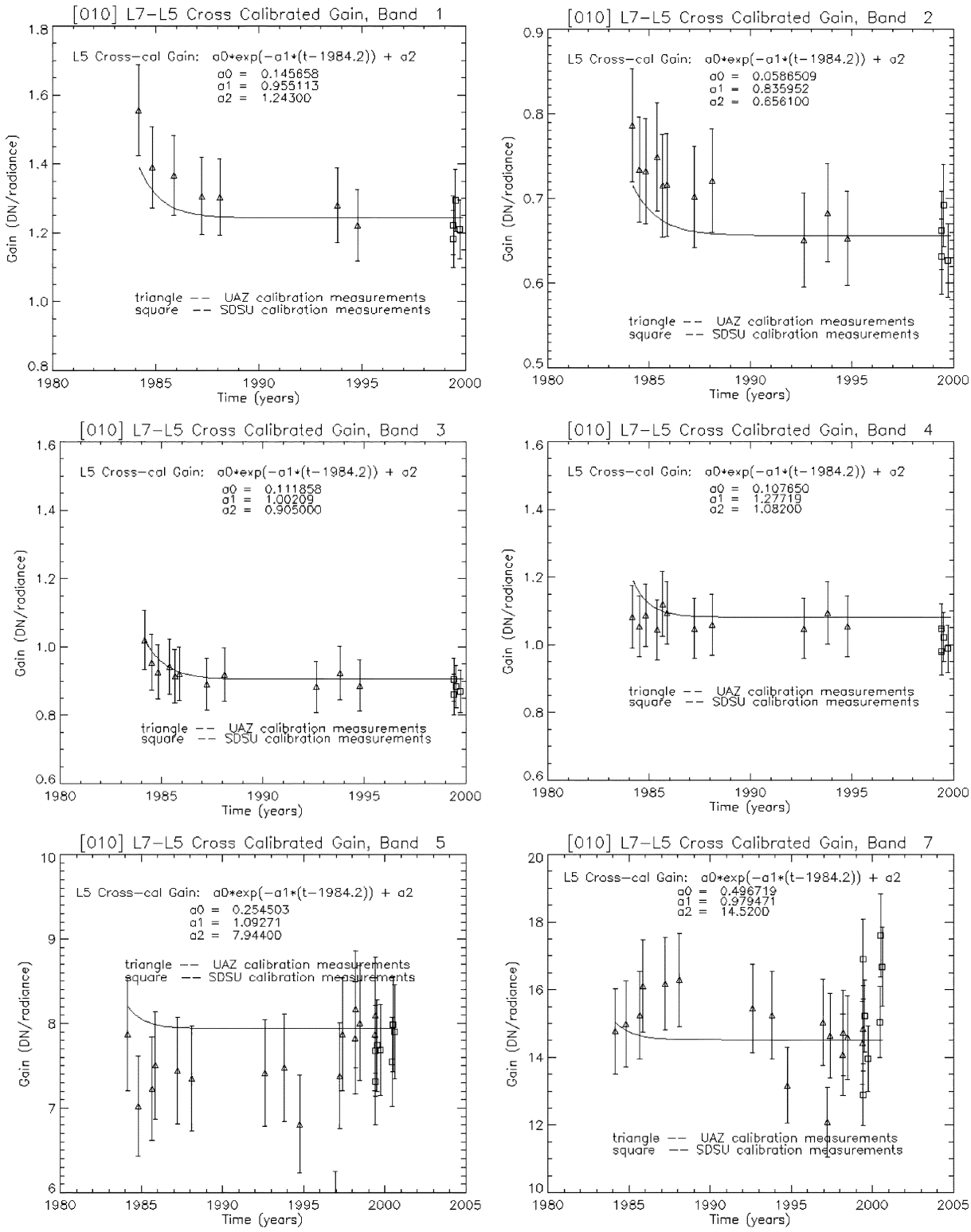

Fig. 3. Lifetime gain plot for the solar reflective bands of L5 TM, tied to L7 ETM+ cross-calibration measurements. DN is digital counts. Radiance is in watts per square meter per sterdian per micron. UAZ is University of Arizona, and SDSU is South Dakota State University.

of the onboard references (lamps, diffusers) through independent means. Vicarious methods provide these independent data and provide insights to drift in the instrument response or the calibration system (IC).

The major advantage of vicarious methods is that the calibration is performed with the system operating in the mode in which it normally collects data. Vicarious approaches take into consideration the full aperture and full optical path calibrations, providing relatively high accuracy in calibration. However, vicarious calibration is labor-intensive, which limits the number of calibrations that can be performed. In addition, calibration can only be performed when the system collects data over the

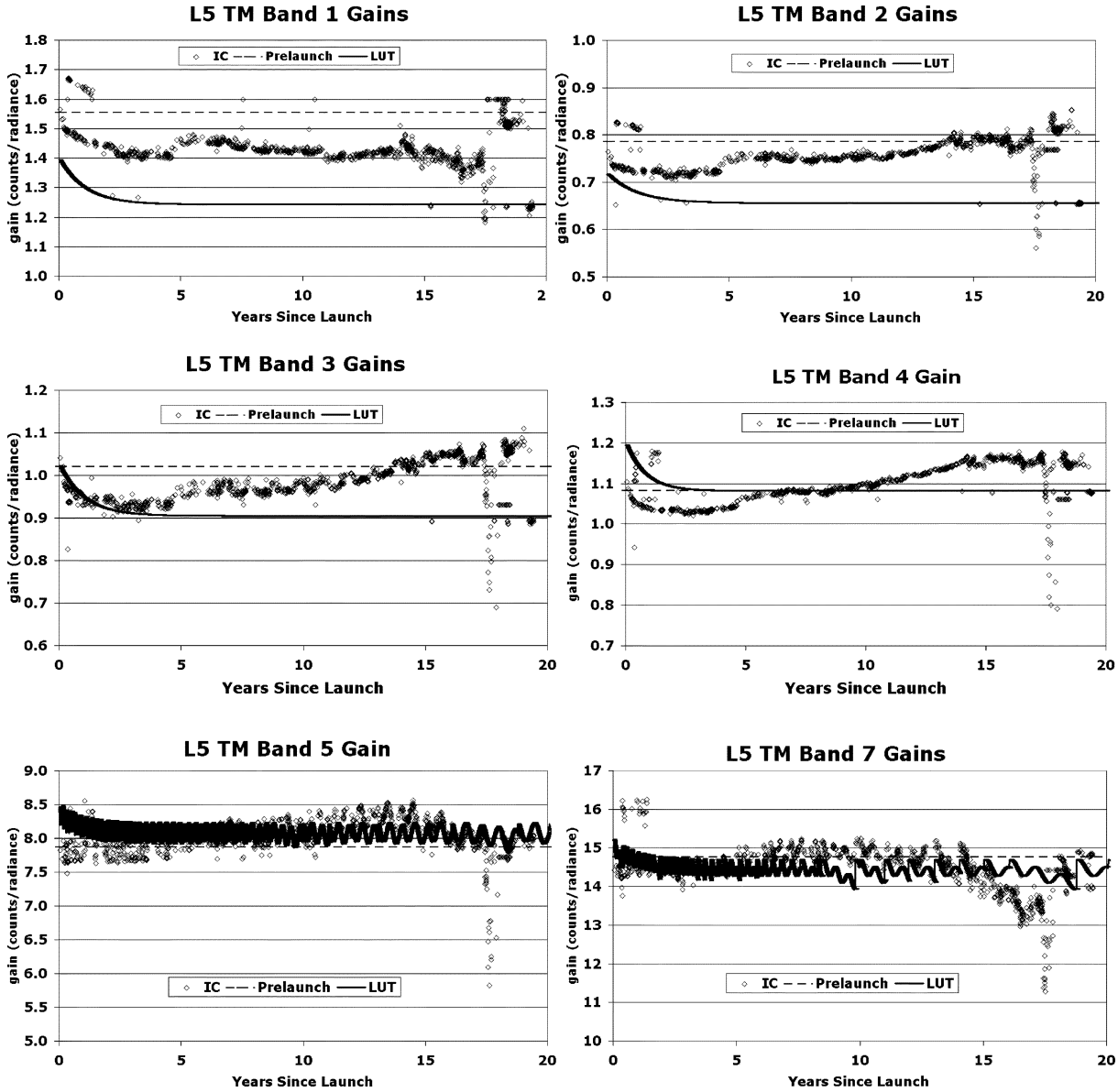

Fig. 4. Lifetime gain plot for the solar reflective bands of L5 TM in radiance units watts per square meter per steradian per micron showing the comparison of the gain generated from IC versus the LUT.

test site. For L5, the maximum number of calibrations possible during a given year, for a given test site, is 22. The actual number will be further reduced due to adverse local weather conditions (i.e., cloud cover obscuring the test site).

Teams from SDSU and the UOA collect vicarious measurements for L5 TM data and use other techniques to calibrate historical data available from the archive. Table III summarizes the gain coefficients obtained from measurements from both teams. The background information and processing methodology have been generated and reported elsewhere. References at the end of this paper provide additional information [2], [9].

C. IC-Based Calibration Gain

NASA/Santa Barbara Research Center (SBRC) developed processing algorithms that estimated detector gain based on the prelaunch calibrated IC lamp responses. The procedure

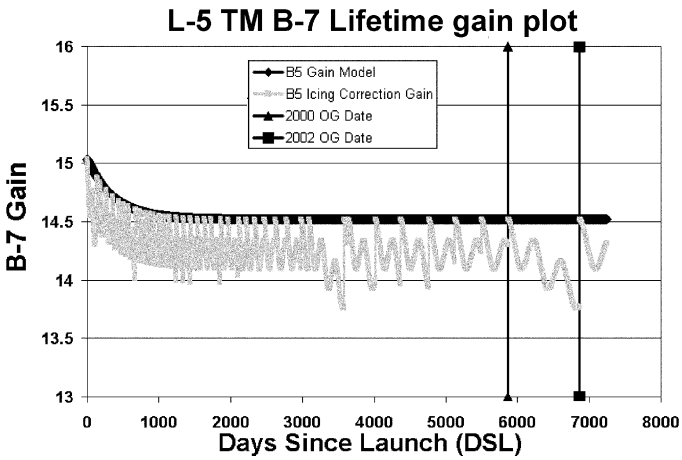

Fig. 5. Lifetime gain plot for band 7 showing the icing corrections. The vertical bar shows an outgassing cycle of 2000.

TABLE VI
L5 TM POSTCALIBRATION DYNAMIC RANGES FOR U.S. PROCESSED NLAPS DATA [4]

Spectral Radiances, Lmin and Lmax in W/(m^2.sr.um)										
Processing Date	From March 1, 1984 To May 4, 2003					After May 5, 2003				
Band	Lmin	Lmax	$G_{rescale}$	$B_{rescale}$	$1/G_{rescale}$	Lmin	Lmax	$G_{rescale}$	$B_{rescale}$	$1/G_{rescale}$
1	-1.52	152.10	0.602431	-1.52	1.66	-1.52	193.0	0.762824	-1.52	1.31
2	-2.84	296.81	1.175100	-2.84	0.85	-2.84	365.0	1.442510	-2.84	0.69
3	-1.17	204.30	0.805765	-1.17	1.24	-1.17	264.0	1.039880	-1.17	0.96
4	-1.51	206.20	0.814549	-1.51	1.23	-1.51	221.0	0.872588	-1.51	1.15
5	-0.37	27.19	0.108078	-0.37	9.25	-0.37	30.2	0.119882	-0.37	8.34
7	-0.15	14.38	0.056980	-0.15	17.55	-0.15	16.5	0.065294	-0.15	15.32

involved regression of lamp responses against the measured radiances for all eight lamp states. The slopes of the regressions represent the gain; the intercepts represent the bias. Constant values of gain and bias are used for each detector for a scene.

Many techniques have been developed to analyze data from the IC over the instrument's lifetime [10]–[14]. Results from IC analysis through 1999 for the solar reflective bands suggest that the L5 TM lifetime radiometric response follows an exponential plus linear model, as shown in Fig. 1. The exponential part seemed to reach an asymptotic limit in 1987 and is considered to be a "true change" in instrument response, likely due (as mentioned earlier) to outgassing from the spectral filters occurring during the first few years after launch.

The subsequent linear increase is considered to be a change in the IC system (i.e., a change in lamp characteristics rather than a true change in instrument response). The L5 TM IC control photodiode is unfiltered. It therefore monitors only total power within its region of spectral sensitivity. The photodiode has to adjust the current going to the lamp to keep this power constant. If the spectral nature of the light output should change (e.g., by yellowing/browning of the lamp envelope), each band will not receive a constant power over time. This could be a contributing factor to some of the changes observed. Hypothetically, the IC lamps may be contaminated in the region viewed by the photodiode in the lamp radiance control system. Such contamination may cause a reduction in measured radiance at the photodiode and drive an increase in overall lamp brightness. Fig. 2 shows the lamp responses for all lamp states from two scenes acquired in 1986 and 2001. It can be seen that the pulses from 2001 are much brighter than the corresponding pulses from the 1986 scene.

Vicarious calibration results suggest a relatively constant response since 1988. The linear increase as seen in the lamp response was not observed in the vicarious calibration results, as shown in Fig. 1(b). Once the linear term was removed from the IC model, agreement between the IC model and the vicarious results improved.

Based on these results, it is currently believed that only the exponential decrease observed in the IC system response and gain model represents a real change in the TM's gain response. The observed linear increase in the IC system response is believed to be a "false" effect, consistent with the understanding that gain response does not increase over time. Thus, in formulating the final temporal characterization, the linear trend is removed from the entire lifetime IC record based on the post-1988 fit. However, the gain calculated using the full IC model introduces error into the radiometric calibration accuracy. Thus, the historical procedure of using the IC to calculate the gain no longer produces the desired calibration; the result is a short-term variation in the apparent gain of the instrument [15].

D. Cross Calibration With L7 ETM+

Early in its mission, the L7 spacecraft was temporarily placed in a "tandem" orbit very close to that of the L5 spacecraft in order to facilitate the establishment of sensor calibration continuity between the ETM+ and TM sensors. During June 1–4, 1999, hundreds of nearly coincident matching scenes were recorded by both the ETM+ and, in cooperation with Space Imaging/EOSAT and IGS's, the TM as well. A cross-calibration method [16] was formulated and implemented to use image pairs from the tandem-orbit configuration period to radiometrically calibrate the solar reflective bands of the TM with respect to the excellent radiometric performance of the ETM+ (to $\pm 3\%$).

Among the matching scenes, only two are known to have coincident ground measurements associated with them. One of the scenes covers the Railroad Valley Playa, NV (RVPN), which is used on a regular basis for sensor radiometric calibration due to its well-characterized relatively stable surface and atmospheric characteristics. Therefore, the RVPN results are considered to be the definitive set of L5 TM gain coefficients for June 1999 (Table IV). Tandem-orbit-based results from other image pairs (not shown) indicate a repeatability of the approach on the order of $\pm 2\%$. For spectral bands 1–4, the estimated uncertainty of this TOA radiance calibration is $\pm 3.6\%$ (one sigma), based on the root sum square of $\pm 3\%$ for ETM+ calibration and $\pm 2\%$ for the tandem-orbit-based cross calibration. Uncertainty estimates have yet to be determined for spectral bands 5 and 7, but experience suggests that they will be approximately 50% greater than the uncertainties in the first four spectral bands. Comparisons with results from independent vicarious calibration methods (Table IV) indicate that the tandem-orbit-based cross calibration is in reasonable agreement with the independent results (to within 2.5% on average and no worse than within 4.4%). A comparison between the 1999 and prelaunch TM gain coefficients is also included in Table IV. The large changes in gain in spectral bands 1–3 underscore the importance of postlaunch calibration updates during the lifetime of the mission [16].

E. Development of Lifetime Calibration Equations

A new formulation for the instrument gain was developed. This formulation models the gain of each band as a time-dependent equation. The model initially consisted of the sum of two terms representing the initial exponential decrease in response (believed to be due to outgassing from the spectral filters) and the linear increase in response and were based on normalized instrument response to reverse scan calibration data from the one lamp (state [010]), with continuous output. The linearly increasing component was not included in the final model. The final model curve was then scaled to the cross-calibration gain estimates for the L7 ETM+ obtained in June 1999, as determined by the tandem-based cross calibration for the RVPN test site [16]. The time-dependent equations for L5 TM gain $G_{\text{new}}(t)$ applicable to raw data take the form

$$G_{\text{new}}(t) = \text{a0} * \exp\left(-\text{a1} * (t - 1984.2)\right) + \text{a2} \qquad (1)$$

where the time t is in decimal years, a0 is a scaling factor for the exponential decrease, a1 is a time constant of the exponential decrease, a2 is a required offset, and 1984.2 refers to "time zero," the date when the earliest lifetime net pulse value was collected. The coefficients a0, a1, and a2 are given in Table V. The gain coefficients in the solar reflective bands are constant and within the accuracy of the vicarious calibration results since approximately 1987. The resulting curves (Fig. 3) are generally consistent with independent lifetime vicarious calibration results obtained by UOA and 1999 estimates obtained by SDSU. For spectral bands 1–4, the lifetime gain curves only fall outside the uncertainty of the vicarious calibration results at the very beginning of the L5 mission in 1984. For spectral bands 5 and 7, the lifetime gain curves do not correspond as well to the independent vicarious calibration measurements.

1) LUT Description: Due to the periodic build up of ice during outgassing cycles as explained in the earlier section, there is an additional $\pm 3\%$ to 5% uncertainty in bands 5 and 7 in any given TM product. The developed thin-film model corrects for most of this effect. The oscillatory nature of this model is such that the $G_{\text{new}}(t)$ for bands 5 and 7 will be better specified in terms of day-specific LUTs. Hence, for consistency, LUTs was used for $G_{\text{new}}(t)$ for all six solar reflective bands.

Fig. 3 shows the final lifetime gain model for L5 TM that has been scaled to the cross-calibration estimates with the L7 ETM+. These gains are generated over the lifetime of the mission and stored in day-specific LUTs. These are referred to as LUT gains in this paper. In the same sense, the gains calculated using IC responses are referred to as IC gains. A comparison of IC versus the LUT gains over the lifetime of the instrument is shown in Fig. 4. The LUT gain plot for the band 7 with incorporated icing corrections are shown in Fig. 5. The Gain Model curve in that figure shows the band 7 gain in absence of the icing problem, and the Icing Correction Gain follows the interference nature of the ice film growth on the CFP window. The vertical lines show the beginnings of the two consecutive outgassing cycles, indicating discontinuities in the interference pattern due to the outgassing process and successful recovery of detector responsivities to the no-ice values.

2) Revised Postcalibration Dynamic Ranges: The L5 TM data products are eight-bit; therefore, the calibrated pixels need to be scaled. The postcalibration dynamic range defines the DN to radiance scaling limits in the Level 1 products. Originally, an identical postcalibration dynamic range was defined for the L4 and L5 TM sensors. The postcalibration dynamic ranges are specified by a maximum radiance LMAX_λ and a minimum radiance LMIN_λ.

Table VI provides band-specific LMAX_λ and LMIN_λ parameters and the corresponding G_{rescale} and B_{rescale} values used at different times for the L5 processing system. The units of spectral radiance are watts per square meter per steradiam per micron

$$G_{\text{rescale}} = \left(\frac{\text{LMAX}_\lambda - \text{LMIN}_\lambda}{Q_{\text{calmax}} - Q_{\text{calmin}}}\right)$$
$$B_{\text{rescale}} = \text{LMIN}_\lambda$$
$$\text{Postcal gain} = \frac{1}{G_{\text{rescale}}}$$

where

- Q_{calmin} minimum quantized calibrated pixel value $(\text{DN} = 0)$ corresponding to LMIN_λ;
- Q_{calmax} maximum quantized calibrated pixel value $(\text{DN} = 255)$ corresponding to LMAX_λ;
- LMIN_λ spectral radiance that is scaled to Q_{calmin} in watts per square meter per steradian per micron;
- LMAX_λ spectral radiance that is scaled to Q_{calmax} in watts per square meters per sterdian per micron.

G_{rescale} (units of watts per square meter per steradian per micron per digital number) and B_{rescale} (units of watts per square meter per steradian per micron) are band-specific rescaling factors typically given in the NLAPS product header file (.h1) and the product generation work order report (.wo) and used for converting the calibrated DNs in L1 products back to at-sensor spectral radiance. Note that gain has been variously defined as radiance per unit DN (typically for the data products) and DN per unit radiance (typically for the instrument), lending confusion to the discussion. When referring to data products, we will call what have typically been called data product gains, e.g., G_{rescale}, scaling factors, and reserve "gain" for the inverse of the scaling factor.

Figs. 6–9 compare the postcalibration gains in relation to the instrument gains being generated by IC and LUT processing for all of the bands. A higher gain implies lower saturation radiance. Generally, the strategy is to set the gain as low as the most sensitive (highest gain) detector in the band will support. Note particularly for bands 1 and 2 that the LUT gains are significantly lower than the IC gains. This means that if the postcalibration range is not changed, then the LUT L1R processing will be forcing more pixels into saturation than the IC processing. This will cause negative impacts in analysis of the bright targets. To avoid this problem, the postcalibration gains were reduced (this means increasing the LMAXs) to remap the calibrated DNs to their new radiance levels. For the other bands, the LUT gains were similar to the IC gains, though some revisions were made.

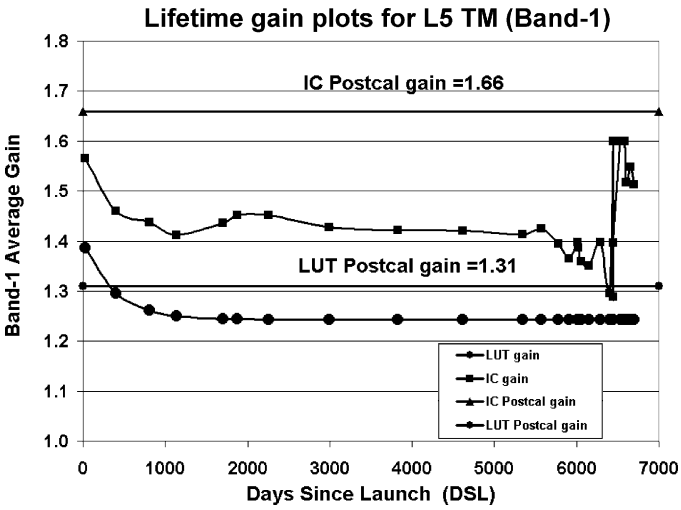

Fig. 6. L5 TM lifetime gain for band 1 with revised postcalibration dynamic ranges.

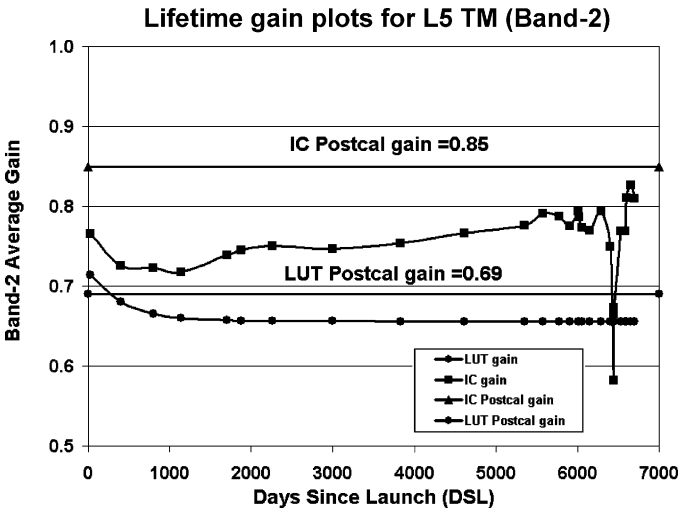

Fig. 7. L5 TM lifetime gain for band 2 with revised postcalibration dynamic ranges.

Beginning May 5, 2003, the new postcalibration dynamic ranges are used for all of the data processed and distributed by the Earth Resources Observation System (EROS) Data Center (EDC) [4]. LMAX was set to be slightly lower than the saturation radiance of the most sensitive detector in the given band. This forces all detectors to "saturate" at the same radiance in the calibrated data product and prevents striping in high-radiance areas. This method allows a fixed postcalibration dynamic range for the life of the mission at the expense of throwing away increasing amounts of data as the gain decreases with time. At all times, however, the data product has the same range. The relative calibration results over the lifetime of the instrument indicate that the maximum variation within a band is $\pm 2.5\%$ from the average. Based on these results, the revised LMAX was chosen 5% above the gain numbers derived from the cross-calibration experiment.

For "early mission" L5 TM data (acquired after launch in 1984 through mid-1985), the change in postcalibration dynamic ranges will introduce high-radiance striping and saturation of

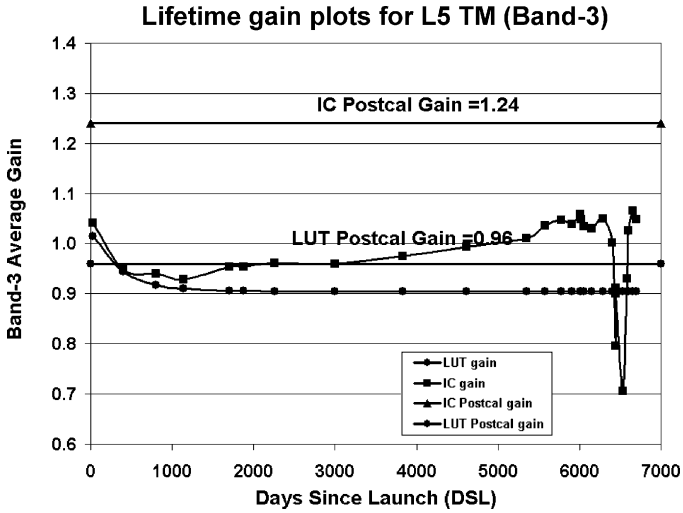

Fig. 8. L5 TM lifetime gain for band 3 with revised postcalibration dynamic ranges.

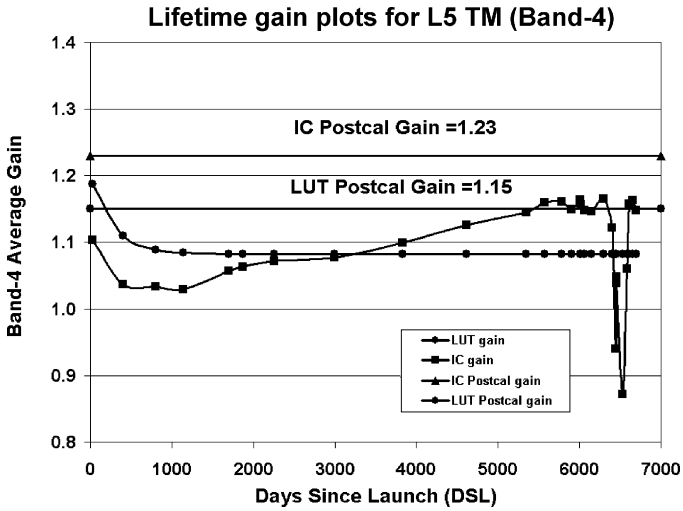

Fig. 9. L5 TM lifetime gain for band 4 with revised postcalibration dynamic ranges.

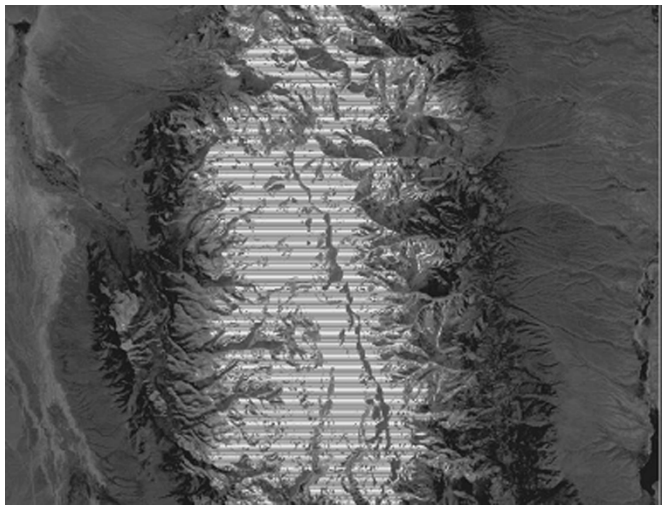

Fig. 10. High-radiance striping for early mission L5 TM data.

calibrated digital counts values below 255, as shown in the Fig. 10. This striping results from each detector saturating at a different DN in the calibrated data products. As shown in

Figs. 6–9, during this time period the postcalibration gain is lower than the instrument LUT gains. Users should consider all the detectors saturated in areas where they observe this high-radiance striping.

The revised postcalibration dynamic ranges are only applicable to the data processed using the LUT gains, and the new LMAXs should not be applied to the data processed using IC gains. The new postcalibration dynamic ranges are considered to be valid only for the L5 TM calibrated products. L4 TM sensor calibration will continue to use the postcallibration dynamic ranges as previously defined.

IV. Improvement in Absolute Calibration Accuracy of L5 With L7

Historically, the L5 TM calibration procedure in NLAPS (adopted from TIPS) used the instrument's response to the IC on a scene-by-scene basis to determine gains and offsets. Effective May 5, 2003, revised L5 TM radiometric calibration procedures and postcalibration dynamic ranges were implemented into the NLAPS system for all of the data processed and distributed by the EDC [4]. The modified approach discontinued use of the IC for the reflective bands (with the exception of the thermal band) and implemented instead a time-dependent calibration LUT. Note that products generated before May 5, 2003 (calibrated with the IC-based gain and converted to radiance using the older LMINs and LMAX values) will not provide the same radiances as those processed since May 5, 2003 (calibrated with the LUT gain and converted to radiance with the new LMINs and LMAXs).

Data continuity within the Landsat program requires consistency in interpretation of image data acquired by different imaging instruments. This section provides another comparison of the reflectance measurements obtained from the "tandem" L5 TM and L7 ETM+ scenes. The goal of this analysis is to show the improvement in consistency of the L5 with L7 imagery achieved by implementation of the LUT approach in L5 data product generation.

Three image pairs acquired in June 1999 were used in this analysis: RVPN having WRS path/row 40/33, Niobrara, NE, having WRS path/row 31/30, and Washington, DC (DC) having WRS path/row 15/33. All scenes were processed to Level 1R (applied radiometric, but no geometric correction). L5 TM scenes were processed using two different calibration procedures through the National Landsat Archive Production System (NLAPS). The first calibration procedure used the IC (based on linear regression through the detector responses to all lamp states collected during a scene acquisition time), and the second approach used the revised and improved calibration procedures. (LUT gains based on a lifetime radiometric calibration gain model) The L7 ETM+ scenes were processed through the Image Assessment System (IAS) using the most current available calibration parameter file (CPF-19).

The L7 and L5 sensors differ in their along-track and across-track pixel sampling. Due to wearing of the bumpers used by the L5 TM scanning mirror, along-track gaps between scans are longer than they are for L7 ETM+. For the same reason and because the ETM+ scan time is slightly longer than the specifica-

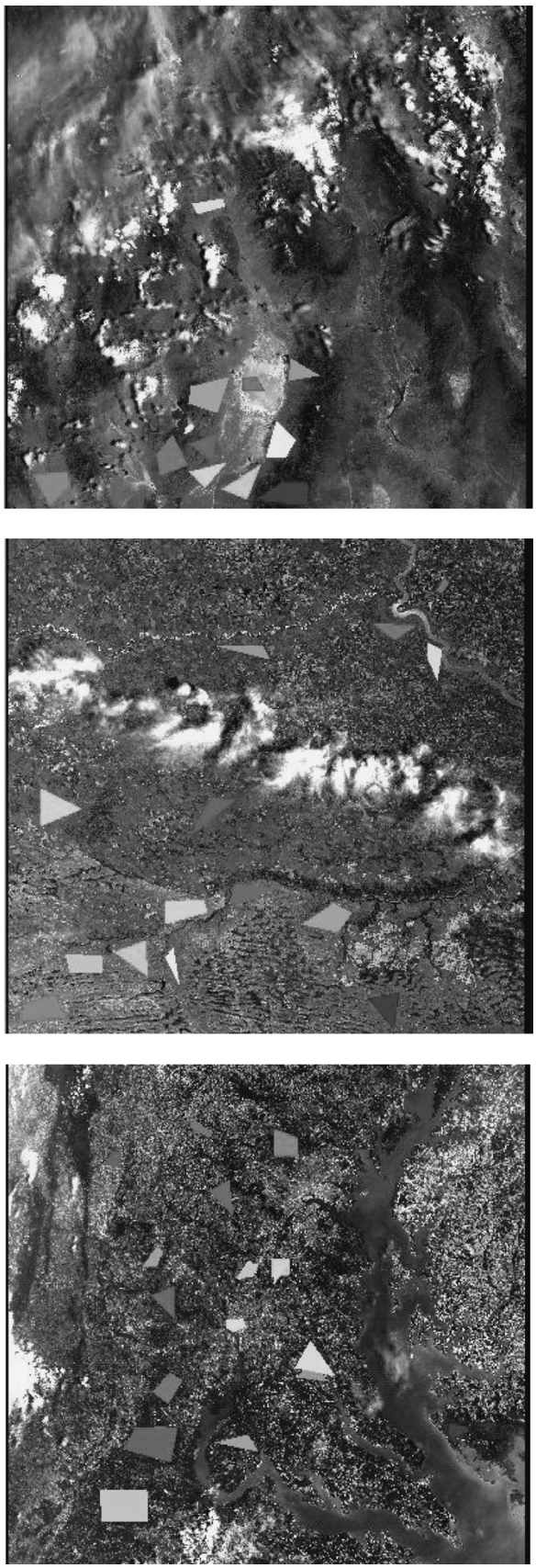

Fig. 11. Areas in common between the ETM+ and TM image pairs.

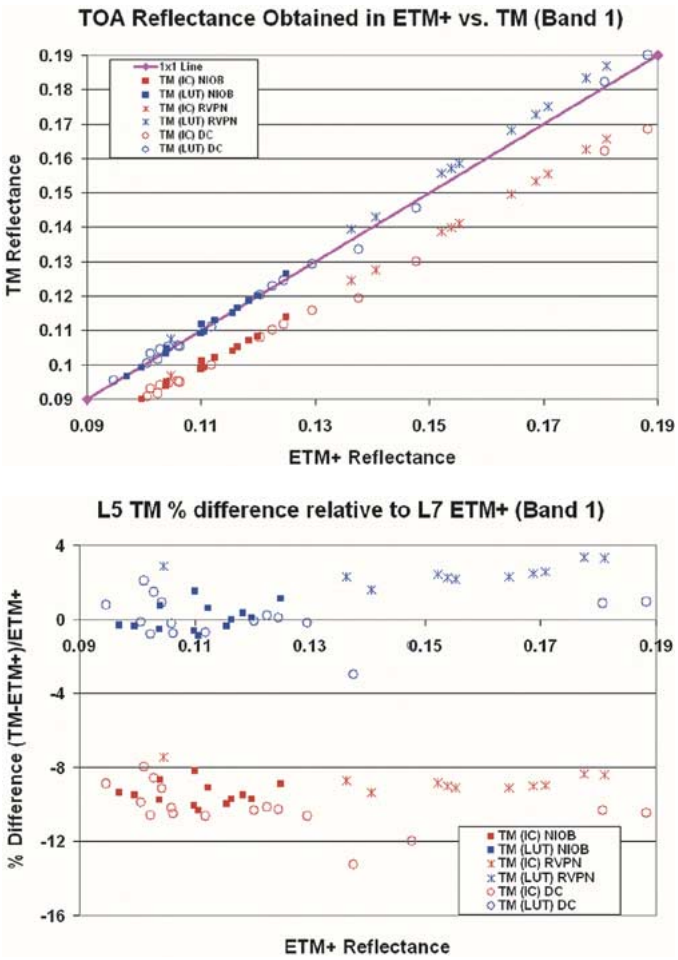

Fig. 12. Comparison of reflectance measurements from large ground regions common to band 1 of both L5 TM and L7 ETM+ instruments.

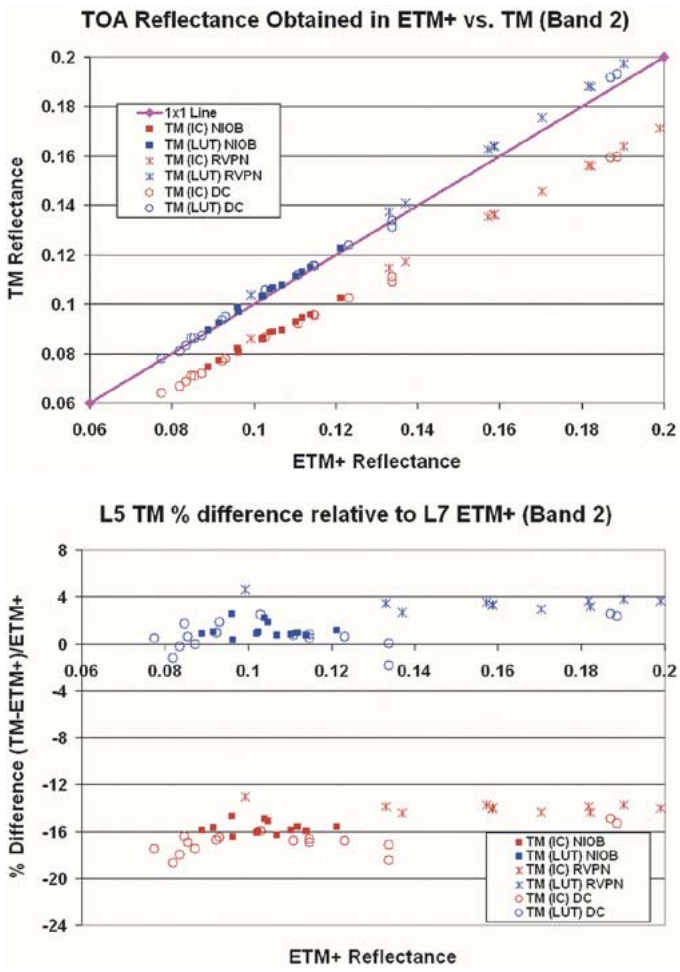

Fig. 13. Comparison of reflectance measurements from large ground regions common to band 2 of both L5 TM and L7 ETM+ instruments.

tion, there are also across-track differences in the ground coverage. In addition, slight mismatches will arise because of the altitude difference. In particular, there is variation in the ETM+ scanning pattern and its effect on the scan line corrector due to the lower-than-nominal orbit during the tandem configuration time period [16]. Due to these reasons, an area common to the two image pairs will have slightly different numbers of pixels. This makes it very difficult to establish sufficient geometric control to facilitate radiometric comparisons on a point-by-point and/or detector-by-detector basis. Therefore, the analysis approach made use of image statistics based on large areas in common between the image pairs (a pair represents an acquisition of a area simultaneously observed by ETM+ and TM systems). These large areas were carefully selected using distinct features common to both the images. In each image pair, the common regions in approximate size of 5–50 km^2 were defined.

Regions of interest were selected within each respective ETM+ and TM. Areas common to the two images in a pair were selected to exclude clouds and cloud shadows. Fig. 11 shows the selected regions that were common to the ETM+ and the respective TM image pairs for the three test sites. From defined regions, mean calibrated DNs were computed and converted to corresponding at-sensor radiances. This is the first and fundamental step in putting image data from multiple sensors and platforms into a common radiometric scale. Further, a reduction in between-scene variability was achieved through normalization for solar irradiance (i.e., converting the spectral radiance, to a planetary or exoatmospheric reflectance). When comparing images from different sensors, there are two advantages to using reflectance instead of radiances. First, the cosine effect of different solar zenith angles due to the time difference between data acquisitions can be removed, and second, it compensates for different values of the exoatmospheric solar irradiances arising from spectral band differences. For this purpose, all of the comparisons were performed on TOA reflectance measurements obtained from ETM+ and TM, respectively.

Results of reflectance comparison for spectral bands 1–4 are presented in Figs. 12–15. The upper plots in each of these figures relate reflectances extracted from L5 TM L1R data to corresponding reflectances obtained from L7 ETM+ data. Each data point on these plots represents an ensemble average of all pixels in a defined region. The one-to-one line points out the idealized perfect agreement between the reflectance measurements obtained from both sensors for a particular band. The lower plots in Figs. 12–15 represent percentage differences in observation

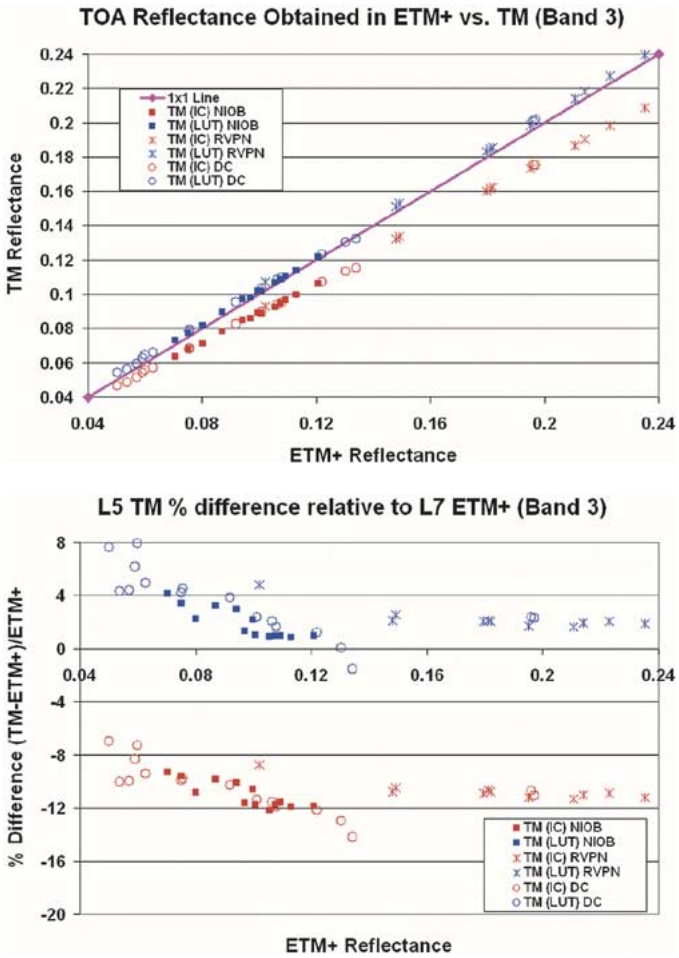

Fig. 14. Comparison of reflectance measurements from large ground regions common to band 3 of both L5 TM and L7 ETM+ instruments.

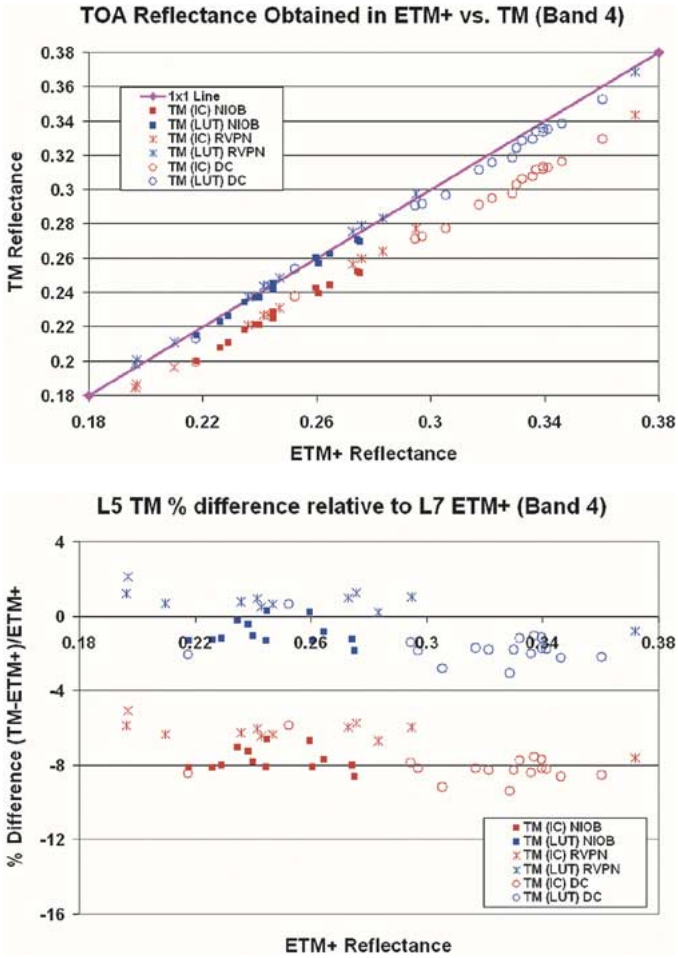

Fig. 15. Comparison of reflectance measurements from large ground regions common to band 4 of both L5 TM and L7 ETM+ instruments.

using the IC and LUT approach in L5 processing relative to L7 data.

The plots clearly indicate a significant improvement toward consistency of L5 data with L7 data achieved using the LUT approach as opposed to the historical calibration procedure. The percentage mean difference in reflectance measurements obtained from the L5 TM relative to ETM+ in band 1 is reduced from about 9.5% to 1.3%, in band 2 from 15.6% to 1.8%, in band 3 from 10.8% to 2.6%, and in band 4 from 7.4% to 1.3% using the LUT calibration approach. Because the imaging of scene pairs was performed only 10–30 min apart, the potential changes in ground and atmospheric conditions should not significantly affect the comparison. The larger differences observed in low-reflectance range in band 3 are probably caused by low SNR in that portion of the instruments' responsivities. In general, no spectral band adjustments were performed, so most of the remaining differences in all bands are accounted to the different relative spectral response profiles of the L7 ETM+ and corresponding L5 TM spectral bands. The consistency between results from the three tandem image pairs is less than 3% for all of the bands, which is well beyond the specified $\pm 6\%$ overall uncertainty for the targets with unknown spectral signatures [16].

V. Conclusion

The Landsat-5 TM sensor has continued to perform well over a period of time far exceeding its expected design life. The 19-year image archive should remain very useful if the revised calibration procedures are used. The revised calibration procedure implemented in May 2003, along with the revised post-calibration dynamic ranges, will provide a data product series that is more self-consistent and more consistent with Landsat-7 ETM+ data. This improvement in the knowledge of the radiometric accuracy of Landsat-5 over its lifetime is indicative of the advancement in the state of the art of on-orbit satellite calibration methods. It is also suggestive of the need for persistent calibrations of an instrument over its lifetime, as well as the need for a variety of calibration methods in order to assess the true radiometric response of an instrument as accurately as possible. Based on the work done with Landsat-5 over the past 20 years, the radiometric fidelity of the instrument has exceeded all expectations and may continue to do so for several more years.

Acknowledgment

The work presented in this paper is the culmination of a multiyear effort of a number of individuals. P. Teillet (Canada

Centre for Remote Sensing) initiated the Landsat TM Calibration Working Group (LTMCALWG) during his sabbatical at the Landsat Project Science Office at Goddard Space Flight Center. The intention of the LTMCALWG charter is to improve the historical radiometric calibration of the pre-L7 instruments.

REFERENCES

[1] B. L. Markham and J. L. Barker, "Spectral characterization of the Landsat Thematic Mapper sensors," *Int. J. Remote Sens.*, vol. 6, pp. 697–716, 1985.

[2] K. J. Thome, B. L. Markham, J. L. Barker, P. L. Slater, and S. F. Biggar, "Radiometric calibration of Landsat," *Photogramm. Eng. Remote Sens.*, vol. 63, pp. 853–858, 1997.

[3] P. M. Teillet, P. M. Helder, T. Ruggles, R. Landry, F. J. Ahern, N. J. Higgs, J. Barsi, G. Chander, B. L. Markham, J. L. Barker, K. J. Thome, J. R. Schott, and F. D. Palluconi, "Toward a definitive calibration record for the Landsat-5 Thematic Mapper anchored to the Landsat-7 radiometric scale," *Can. J. Remote Sens.*, vol. 30, no. 4, pp. 631–643, Aug. 2004.

[4] G. Chander and B. L. Markham, "Revised Landsat-5 TM radiometric calibration procedures, and postcalibration dynamic ranges," *IEEE Trans. Geosci. Remote Sensing*, vol. 41, pp. 2674–2677, Nov. 2003.

[5] B. L. Markham and J. L. Barker, "Landsat MSS and TM post-calibration dynamic ranges, exoatmospheric reflectances and at-satellite temperatures,", vol. 1, EOSAT Landsat Tech. Notes, Aug. 1986.

[6] D. L. Helder and T. A. Ruggles, "Landsat Thematic Mapper reflective-band radiometric artifacts," *IEEE Trans. Geosci. Remote Sensing*, vol. 42, pp. 2704–2716, Dec. 2004.

[7] G. Chander, D. L. Helder, and W. C. Boncyk, "Landsat-4/5 band-6 relative radiometry," *IEEE Trans. Geosci. Remote Sensing*, vol. 40, pp. 206–210, Jan. 2002.

[8] NASA GSFC, "Landsat to ground station interface description," Goddard Space Flight Center, Greenbelt, MD, Rev. 9, Jan. 1986.

[9] K. J. Thome, B. G. Crowther, and S. F. Biggar, "Reflectance and irradiance based calibration of Landsat-5 Thematic Mapper," *Can. J. Remote Sens.*, vol. 23, pp. 309–317, 1997.

[10] D. L. Helder, "A radiometric calibration archive for Landsat TM," *Proc. SPIE*, vol. 2758, pp. 273–284, June 1996.

[11] D. L. Helder, J. L. Barker, W. C. Boncyk, and B. L. Markham, "Short term calibration of Landsat TM: Recent findings and suggested techniques," in *Proc. IGARSS*, Lincoln, NE, 1996, pp. 1286–1289.

[12] D. L. Helder, W. C. Boncyk, and R. Morfitt, "Absolute calibration of the Landsat Thematic Mapper using the internal calibrator," in *Proc. IGARSS*, Seattle, WA, 1998, pp. 2716–2718.

[13] B. L. Markham, J. C. Seiferth, J. Smid, and J. L. Barker, "Lifetime responsivity behavior of the Landsat-5 Thematic Mapper," *Proc. SPIE*, vol. 3427, pp. 420–431, 1998.

[14] P. M. Teillet, D. L. Helder, B. L. Markham, J. L. Barker, K. J. Thome, R. Morfitt, J. R. Schott, and F. D. Palluconi, "A lifetime radiometric calibration record for the Landsat Thematic Mapper," in *Proc. Can. Symp. Remote Sensing*, Aug. 2001, pp. 17–25.

[15] South Dakota State Univ. (SDSU). Radiometric characterization and calibration of Landsat-4/5 Thematic Mappers. Image Processing Lab, South Dakota State Univ., Brookings. [Online]. Available: http://iplab2out.sdstate.edu/projects/landsat45/tmcal/index.html.

[16] P. M. Teillet, J. L. Barker, B. L. Markham, R. R. Irish, G. Fedosejevs, and J. C. Storey, "Radiometric cross-calibration of the Landsat-7 ETM+ and Landsat-5 TM sensors based on tandem data sets," *Remote Sens. Environ.*, vol. 78, no. 1–2, pp. 39–54, 2001.

Gyanesh Chander received the M.S. degree in electrical engineering from South Dakota State University, Brookings, in 2001.

He is currently a Scientist with Science Applications International Corporation (SAIC) at the Earth Resources Observation System Data Center, U.S. Geological Survey, Sioux Falls, SD. He works on radiometric characterization and calibration of satellites and airborne instruments.

Dennis L. Helder (S'88–M'90) received the B.S. degrees in animal science and electrical engineering, the M.S. degree in electrical engineering from South Dakota State University, Brookings, and the Ph.D. degree in electrical engineering from North Dakota State University, Fargo, in 1979, 1980, 1985, and 1991, respectively.

For the past ten years, he has worked extensively with the Earth Resources Observation System Data Center, the National Aeronautics and Space Administration's Goddard Space Flight Center (GSFC), and Stennis Space Center in the area of radiometric, geometric, and spatial calibration of satellite imagery. Other activities include consulting, membership on the international Committee of Earth Observation Satellites Infrared, Visible, and Optical Sensor's subcommittee, a Visiting Scientist appointment at GSFC, development of the Landsat-7 image assessment system with GSFC, and design of aircraft imaging systems.

Brian L. Markham (M'04) received the B.S. degree with a specialization in natural resources and the M.S. degree in remote sensing from Cornell University, Ithaca, NY, in 1976 and 1978, respectively, and the M.S. degree in applied physics from The Johns Hopkins University, Baltimore, MD, in 1996.

He has been a Physical Scientist at the National Aeronautics and Space Administration Goddard Space Flight Center, Greenbelt, MD, since 1978. His research has focused on characterizing the radiometric properties of ground, aircraft, and satellite sensor systems, as well as characterizing atmospheric aerosol optical properties for correction of optical remote sensing data. He has been the Landsat Calibration Scientist since 1993, where he has been involved in the prelaunch and on-orbit radiometric characterization and calibration of the Landsat-7 ETM+ sensor.

James D. Dewald (S'92–M'92) received the B.S. degree in electrical engineering and the M.S. degree in engineering from South Dakota State University (SDSU), Brookings, in 1992 and 1994, respectively.

He is currently with the Department of Electrical Engineering and Computer Science, SDSU, in both an instructional and research capacity. His current research activities include radiometric sensor calibration and application of remotely sensed data for agriculture purposes.

Ed Kaita received the B.S. degree in physics and astronomy from the State University of New York, Stony Brook, and the M.S. degree in physics from the University of Kentucky, Lexington.

He has worked within the National Aeronautics and Space Administration Goddard Space Flight Center contractor community for the past two decades supporting instrument and data calibration activities for the Hubble Space Telescope, the Cosmological Background Explorer Satellite, and most recently the Landsat-7 project.

Kurtis J. Thome received the B.S. degree in meteorology from Texas A&M University, College Station, and the M.S. and Ph.D. degrees in atmospheric sciences from the University of Arizona, Tucson.

He is currently an Associate Professor of optical sciences at the University of Arizona, where he is the head of the Remote Sensing Group. He has served as a member of the Landsat-7, ASTER, and MODIS science teams. His current research is focused on the vicarious calibration of earth-imaging sensors and related studies in atmospheric remote sensing, radiative transfer, and satellite atmospheric correction

Esad Micijevic received the B.S. degree in electrical engineering from the University of Zagreb, Zagreb, Croatia, and the M.S. degree in engineering from South Dakota State University, Brookings.

He has been working on Landsat radiometric and geometric characterization and calibration since 2001 and has been with Science Applications International, Corporation, EROS Data Center, Sioux Falls, SD, since 2003.

Timothy A. Ruggles (S'91–M'92) received the B.S. degree in engineering physics/electrical engineering and the M.S. degree in electrical engineering from South Dakota State University (SDSU), Brookings, in 1992 and 1996, respectively.

He is currently an Imaging Engineer with the Image Processing Laboratory, SDSU, working on issues related to radiometric characterization and calibration of earth imaging sensors such as the Landsat-5 Thematic Mapper and the EO-1 Advanced Land Imager.